Two component statistical model of coherent radar sea clutter

Stephen Bocquet
Defence Science and Technology Group, Australia
stephen.bocquet@dst.defence.gov.au

***Abstract*— A new two component compound Gaussian model is proposed for coherent radar sea clutter, with each component having its own spatial correlation. One component represents Bragg scattering from capillary waves, modulated in both frequency and intensity by gravity waves, and the other fast scattering from breaking waves. The intensity of each component is represented by an independent gamma variate with its own scale and shape parameter, with the overall texture distributed as the sum of these two gamma variates. The model is compared to data collected at medium grazing angles with the DST Ingara airborne X-band radar. It is able to explain many of the distinctive features of coherent radar sea clutter.**

Keywords—radar; sea clutter; Doppler spectrum; compound Gaussian

I. INTRODUCTION

Modelling and simulation of radar sea-clutter is important for evaluating radar detection algorithms and to stimulate radar processors during development and testing. The Doppler spectrum of sea clutter plays a key role in determining the statistics which are important for coherent processing. Producing simulated sea clutter requires accurate representation of a number of characteristics including the amplitude statistics, short-term temporal correlation (including that represented by Doppler spectra) and spatial and longer-term temporal variations. It must also represent the variation of range and azimuth over time as observed from a wide-area surveillance radar and model the effect of platform motion on the radar returns.

In the literature, the mean Doppler spectrum is often characterised by a single Gaussian component with an offset and spread [1], but a single component with Gaussian statistics is unable to reproduce the observed temporal and spatial variation in the Doppler spectrum. This variability affects the edges of the spectrum most, and is typically asymmetric, with one side of the spectrum having greater variability than the other [2]. Watts [3] showed how a single component with compound K-distributed statistics and a correlation between Doppler shift and intensity can model this asymmetric variability. The correlation gives out at high intensities, so a modification that takes this into account was proposed [4],[5], with a second component that only becomes apparent at high intensity.

Walker [6],[7] identified three distinct components in sea clutter: (1) Bragg scattering from capillary waves, modulated by long wavelength gravity waves; (2) scattering from whitecaps, and (3) specular backscatter from wave crests just prior to breaking. It is difficult to clearly identify all three components in the Doppler spectrum of sea clutter, but the mean spectrum can be fitted to separate Bragg and fast scatter components [8]. Although the existence of two or three components in the Doppler spectrum is generally recognized, models for the spatial and longer-term temporal variations have relied on one correlated variate representing the local clutter power, with a gamma [3]-[5],[9] or inverse gamma [10] distribution. Recently McDonald and Cerutti-Maori (MCM) [11],[12] proposed a two component model where the spatial variability in the Bragg component is derived from a regular wave pattern, but there is no Doppler-intensity correlation. Their model is compared to data from the DST Group Ingara radar in [13].

In this paper a new two component model is proposed, with a separate spatial correlation for each component. The intensity of each component is represented by an independent gamma variate with its own scale and shape parameter. The overall local clutter power or texture is distributed as the sum of these two gamma variates. The Bragg component, centered near zero Doppler, accounts for most of the power in the spectrum but only a relatively small part of the variance. The second component, representing fast scattering processes, is weaker but accounts for most of the variance. The fast scatter component is offset in Doppler, making the overall spectrum asymmetric. The model is compared to data from the Ingara radar, with three different, but complementary, methods used to separate the two components and estimate parameters. In Section II, the two components are separated by simultaneous fitting of the Doppler and variance spectra. In Section III, a new model is proposed for the texture, the distribution for the sum of two independent gamma variates, denoted G2. Fitting the texture probability density function (PDF) to the G2 model gives estimates of the intensities and gamma shape parameters of the two components. The range variation of the two components is difficult to separate, but this is achieved in Section IV for HH polarization in the up swell direction, by cyclic averaging of the Doppler spectrum over the swell wavelength. The Bragg component shows sinusoidal variation in both intensity and Doppler frequency. These variations are almost in phase, and provide an explanation for the observed correlation between the spectrum center frequency and intensity. Further work is needed to more fully validate the model and apply it to the simulation of sea clutter.

II. Doppler and Variance Spectra

Data collected in August 2004 off the coast of Port Lincoln, South Australia, with the DST Group Ingara X-band airborne radar is analyzed. The data was collected in a spotlight mode, with the radar beam pointing broadside and the aircraft following a circular flight path. A dual polarized mode was used, where the radar transmitted with either horizontal or vertical polarization and received both polarizations. More detail on the radar and data collection can be found in [8].

The data has been analyzed for different look directions in azimuth, but the results presented here are confined to the upwind look direction. The wind and swell directions coincide, so upwind is also up swell. Two seconds of data was selected in the upwind look direction and a fast Fourier transform applied to obtain the Doppler spectrum, using a 64 pulse coherent processing interval (CPI) and 55 dB Dolph-Chebyshev window. The pulse repetition frequency (PRF) is 578 Hz and the range resolution 0.73 m. The selected data spans 6° in grazing angle, from 31° to 37°, or 530 m in range. Fig. 1 shows the range-Doppler image for HH polarization, looking upwind. The image is an average of two seconds of data (18 CPI), so as to highlight the features of the Doppler spectrum that are periodic in range. The mean Doppler spectrum is shown in Fig. 2, with the noise background subtracted, for HH and HV polarizations.

The second intensity moment gives information about the variability of the power in each Doppler bin. This information can be presented in several different ways. Miller [2] used the coefficient of variation (the ratio of the standard deviation to the mean). Watts [3] used the normalized second intensity moment and also calculated an effective shape parameter for each Doppler bin, as did MCM [11]. Here we calculate the variance of the local clutter power in each Doppler bin, and normalize the resulting variance spectrum to unit area. The advantage of doing this is that the total variance in each bin is the sum of the variances from the individual components, assuming they are independent, whereas the other statistics do not have this linear property. If ζ is the clutter speckle plus noise power, the variance in the local clutter power z is

$$\sigma_z^2 = \langle z^2 \rangle - \langle z \rangle^2 = \tfrac{1}{2}\langle \zeta^2 \rangle - \langle \zeta \rangle^2 , \qquad (1)$$

where $\langle\rangle$ denotes the mean.

The variance spectrum for a component with a Gaussian power spectral density (PSD), with center frequency f_0 and standard deviation σ, is obtained as follows. If the component intensity x is gamma distributed, with shape ν and unit mean, the intensity PDF is

$$P_c(x) = \frac{\nu^\nu}{\Gamma(\nu)} x^{\nu-1} e^{-\nu x} . \qquad (2)$$

The spectrum moments are

$$S_n(f \mid f_0, \sigma) = \int_0^\infty \left(\frac{x}{\sqrt{2\pi}\sigma} \exp\left(-\frac{(f-f_0)^2}{2\sigma^2} \right) \right)^n P_c(x)\, dx \qquad (3)$$

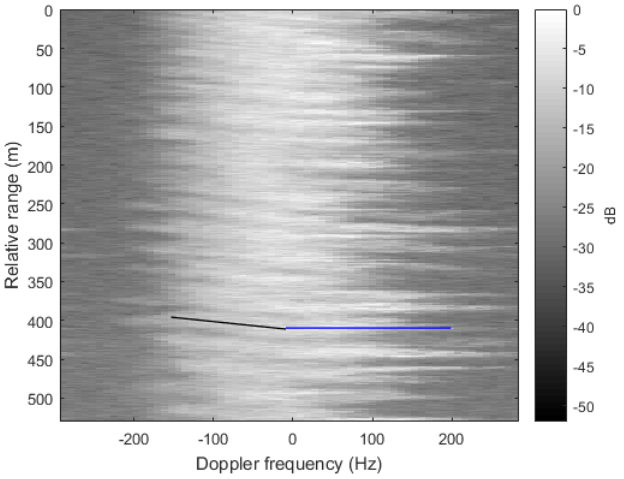

Fig. 1. Range-Doppler image for HH polarization looking up swell, averaged over 18 CPIs. Black and blue lines indicate the range-Doppler variation of the peak intensity for the Bragg and fast scattering components respectively.

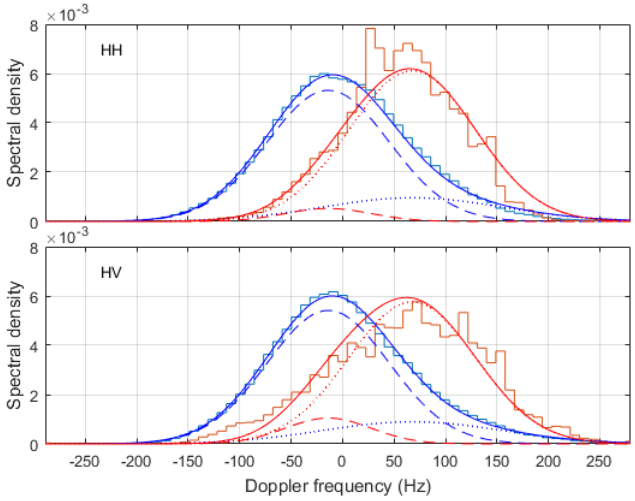

Fig. 2. Doppler (blue) and variance (red) spectra, for HH and HV polarizations looking up swell, fitted to two Gaussian components. Staircase plots, data; solid curves, overall fit; dashed curves, Bragg component; dotted curves, fast scattering component.

The variance spectrum can be calculated from the first two moments as

$$\begin{aligned} V(f \mid f_0, \sigma) &= S_2(f \mid f_0, \sigma) - \left(S_1(f \mid f_0, \sigma) \right)^2 \\ &= \frac{1}{\nu} \left(S_1(f \mid f_0, \sigma) \right)^2 \\ &= \frac{1}{2\sqrt{\pi}\sigma\nu} S_1\left(f \mid f_0, \frac{\sigma}{\sqrt{2}} \right). \end{aligned} \qquad (4)$$

The variance spectrum is also Gaussian in shape, but narrower by a factor of √2. The shape parameter ν is obtained as the ratio of the component power squared to the variance. Simultaneous fitting of the Doppler and variance spectra to two Gaussian components (Fig. 2) provides estimates of their center frequencies, widths, intensities and shape parameters (Table I).

p_1 is the proportion of the total intensity due to the Bragg component. The two components are assumed to be independent, with zero covariance, but this assumption is reexamined at the end of Section IV C. The Bragg component, centered near zero Doppler frequency, has very low variance, while the fast component has a higher center frequency and greater variance. Spectra for the two receive polarizations were fitted to the same center frequencies and widths. In dual polarization mode, transmission of horizontal or vertical polarization occurred at different times, so the HV and VH spectra are not identical.

TABLE I. PARAMETERS FROM TWO COMPONENT FITS TO DOPPLER AND VARIANCE SPECTRA

Pol.	f_1 (Hz)	f_2 (Hz)	σ_1 (Hz)	σ_2 (Hz)	p_1	ν_1	ν_2
HH	-13.9	67.8	59.3	87.1	0.79	234	0.97
HV					0.80	259	1.91
VV	-11.1	63.8	59.6	98.7	0.90	105	1.59
VH					0.80	6×10^{14}	1.51

III. G2 TEXTURE MODEL

If the intensities of the two Doppler spectrum components are modeled with independent gamma variates, each with its own scale and shape parameter, the overall texture consists of the sum of the two gamma variates, with the PDF

$$\begin{aligned} P(z) &= \frac{b_1^{\nu_1} b_2^{\nu_2}}{\Gamma(\nu_1)\Gamma(\nu_2)} \int_0^z \exp\left(-b_1(z-y)-b_2 y\right)(z-y)^{\nu_1-1} y^{\nu_2-1} dy \\ &= \frac{b_1^{\nu_1} b_2^{\nu_2} z^{\nu_1+\nu_2-1}}{\Gamma(\nu_1)\Gamma(\nu_2)} \mathrm{e}^{-b_1 z} \int_0^1 \exp\left((b_1-b_2)zt\right)(1-t)^{\nu_1-1} t^{\nu_2-1} dt \\ &= \frac{b_1^{\nu_1} b_2^{\nu_2} z^{\nu_1+\nu_2-1}}{\Gamma(\nu_1+\nu_2)} \mathrm{e}^{-b_1 z} \, {}_1F_1\left(\nu_2, \nu_1+\nu_2; (b_1-b_2)z\right) \end{aligned} \tag{5}$$

The shape and scale parameters of the two components are respectively ν_1, ν_2 and b_1, b_2. ${}_1F_1(\cdot)$ is the confluent hypergeometric function. For brevity we refer to this distribution of the sum of two gamma variates as G2. The intensity moment of order n is

$$\begin{aligned} \langle z^n \rangle &= \int_0^\infty z^n P(z)\, dz \\ &= b_1^{-\nu_2-n} b_2^{\nu_2} \frac{\Gamma(\nu_1+\nu_2+n)}{\Gamma(\nu_1+\nu_2)} \, {}_2F_1\left(\nu_2, \nu_1+\nu_2+n; \nu_1+\nu_2; \frac{b_1-b_2}{b_1}\right) \end{aligned} \tag{6}$$

The mean and variance are

$$\langle z \rangle = \frac{\nu_1}{b_1} + \frac{\nu_2}{b_2}, \qquad \langle z^2 \rangle - \langle z \rangle^2 = \frac{\nu_1}{b_1^2} + \frac{\nu_2}{b_2^2}. \tag{7}$$

As expected for the sum of independent variates, the mean is the sum of the means and the variance the sum of the variances from the individual distributions. If the distribution is normalized so that $\langle z \rangle = 1$, $b_1 = \nu_1/p_1$ and $b_2 = \nu_2/(1-p_1)$. Parameter estimation for the G2 distribution presents some difficulties, with four parameters to estimate. Two parameters can be estimated from the mean and variance, with the remaining two obtained by nonlinear least squares fitting of the log PDF. Estimators that involve log moments are intractable for the G2 distribution, because they involve order derivatives of the hypergeometric function in (6).

Fig. 3 shows the texture distribution fitted to the G2 model. Three other distributions are shown for comparison: the gamma, inverse gamma and gamma plus constant distributions. The $z \log z$ estimator was used to estimate the parameters. In the case of the gamma plus constant distribution, the $z \log z$ estimator is the one for the K plus Rayleigh distribution [14] with the number of looks set to infinity. The texture distribution varies with polarization as shown in Fig. 3, but there is very little variation with azimuth. Table II has the parameters from the distribution fits in Fig. 3.

A compound G2 distribution can be constructed from the G2 texture model, with the PDF

$$P(\zeta \mid p_n) = \int_0^\infty \frac{1}{z+p_n} \exp\left(-\frac{\zeta}{z+p_n}\right) P(z)\, dz \tag{8}$$

for the clutter speckle plus noise power ζ. There is no analytic solution to the integral (8), even if the noise power p_n is neglected, so numerical integration must be used. The compound G2 model fits the time domain intensity PDF quite well, but there is insufficient space to present the results here.

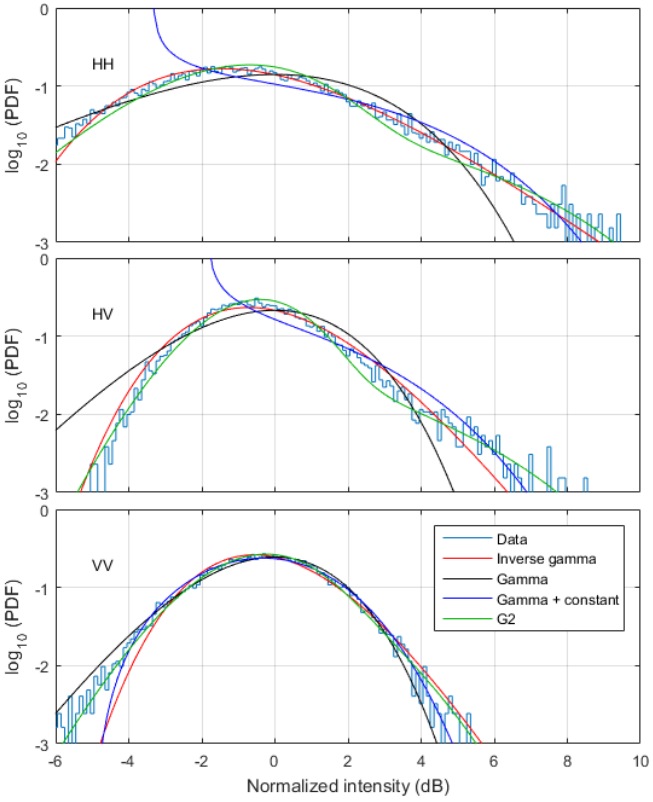

Fig. 3. Texture PDF (staircase plots) fitted to different models (curves), three polarizations looking up swell.

TABLE II. TEXTURE PDF FIT PARAMETERS, UP SWELL

	Gamma	Inverse gamma	Gamma + constant			G2		
Pol.	***shape***	***shape***	***shape***	***scale***	***const.***	v_1	v_2	p_1
HH	2.46	3.46	0.48	0.90	0.46	5.04	0.084	0.80
HV	5.59	6.59	0.48	1.38	0.65	12.24	0.070	0.89
VV	7.29	8.29	3.21	4.68	0.31	10.06	0.27	0.86

IV. SPATIAL CORRELATION

A. Doppler Parameters

The upper plot in Fig. 4 shows the spatial correlation in the Doppler spectrum intensity, centroid and width, for HH polarization looking up swell. There is a dominant wavelength of 30 m, as reported previously [10]. The lower plot in Fig. 4 shows the cross-correlations between the intensity and centroid and between the intensity and spectral width. The intensity and centroid are in phase with one another, whereas the spectral width is out of phase. This has been observed previously in coherent sea clutter data from a land based radar [15], [16].

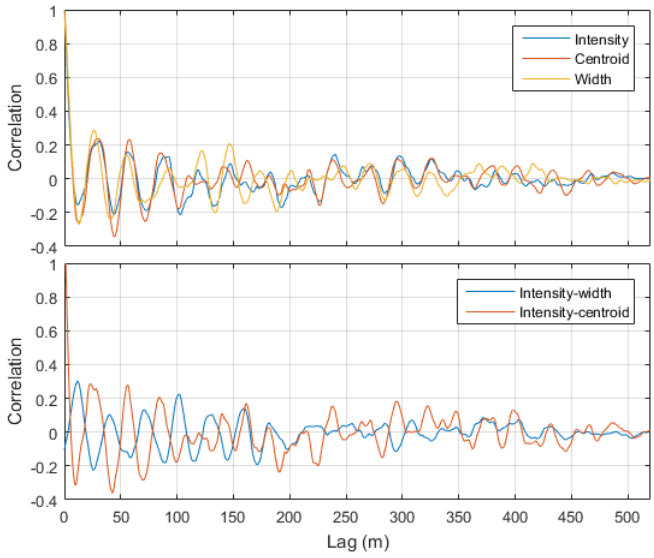

Fig. 4. (Top) Range autocorrelation of the Doppler spectrum intensity, centroid and width, averaged over 18 CPI (2 seconds), for HH polarization looking up swell. (Bottom) Cross-correlations between Doppler spectrum intensity and width, and between intensity and centroid.

The 2D PSD in wavenumber and Doppler frequency for the up swell HH data (Fig. 5) has a prominent ridge at a wavenumber of 0.033 m^{-1}, indicating that the 30 m swell wavelength is present across most of the Doppler spectrum. The range-Doppler image (Fig. 1) has a distinctive herringbone pattern, with the peak positions in the left side of the spectrum varying in both range and Doppler, whereas on the right they do not vary in range. The estimated phase across the Doppler spectrum is shown in Fig. 6. The peak intensity position overlaid on the range-Doppler image in Fig. 1 is found by subtracting the phase from an integer multiple of the swell wavelength. Comparison with the two components in the mean Doppler spectrum (Fig. 2) suggests that the Bragg component peaks vary in both range and Doppler, but the fast component peaks are spread in Doppler only. MCM [12] make a similar observation from their data.

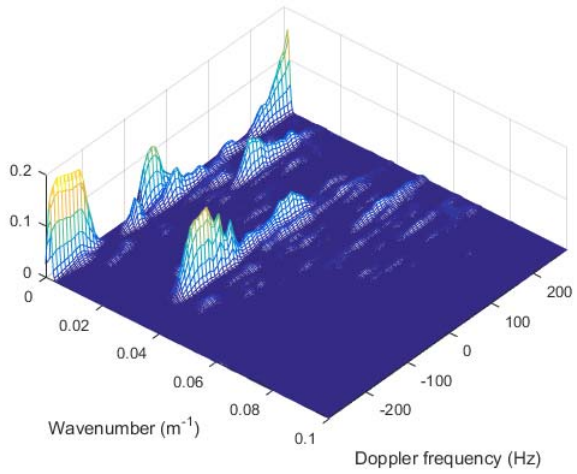

Fig. 5. PSD over spatial wavenumber and Doppler frequency, for HH polarization looking up swell.

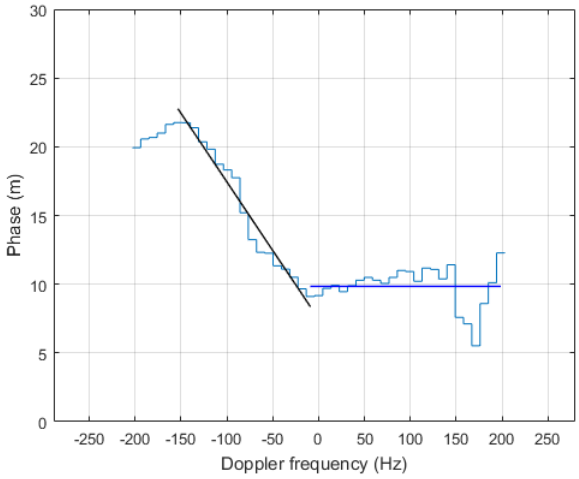

Fig. 6. Relative phase of peak intensity across the Doppler spectrum, for HH polarization looking upswell. Black regression line indicates the varying phase in the Bragg component. Blue line shows the constant phase for the fast scattering component.

B. Doppler-Intensity Correlation

There is a clear correlation between the Doppler spectrum center frequency and intensity, albeit with considerable scatter (Fig. 7). This correlation depends on both look direction and polarization, being strongest for HH polarization up or down swell, but very small in the cross-swell directions and very small for VV polarization in any look direction [4]. Here it is proposed that the correlation is a characteristic of the Bragg component, because both the amplitude and frequency of the backscatter from the capillary waves on the surface are modulated by the gravity waves or swell [16], whereas the amplitude of the fast scattering events is largely independent of their Doppler frequency.

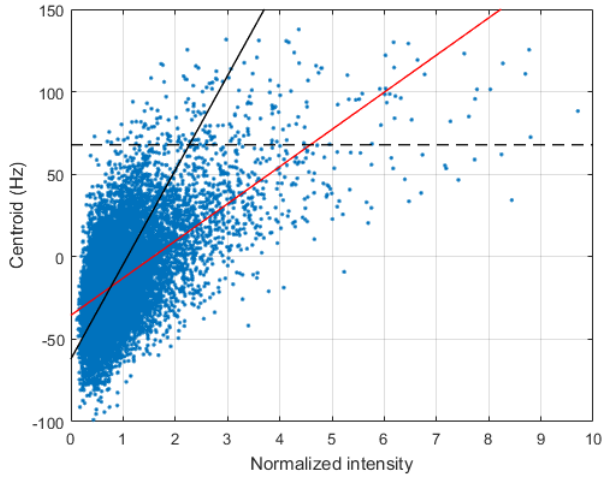

Fig. 7. Correlation between the Doppler spectrum centroid and intensity, for HH polarization, looking up swell. The red line is a least squares fit to the data. The black solid line shows the correlation between the center frequency and intensity of the Bragg component and the dashed line indicates the mean center frequency of the fast component.

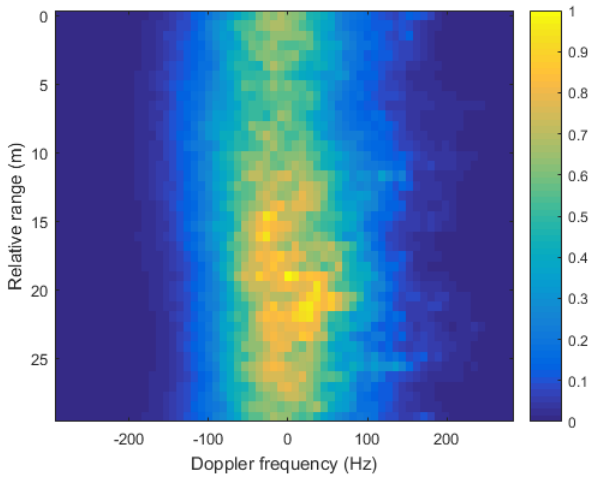

Fig. 8. Range-Doppler image for HH polarization looking up swell, averaged in range on a 30 m cycle.

C. *Separating the Spatial Correlations*

The overlap of the two components makes their range variation difficult to separate, but some progress can be made if the Doppler spectrum is averaged in range on a 30 m, or 41 range bin, cycle (Fig. 8). The range variation of intensity, centroid and bandwidth for this averaged spectrum is shown on the left hand side of Fig. 9. Two Gaussian components with intensities I_1,I_2, center frequencies f_1,f_2 and standard deviations σ_1, σ_2 have a mean f_0 and variance σ^2, with

$$f_0 = p_1 f_1 + (1-p_1) f_2$$
$$\sigma^2 = p_1(1-p_1)(f_1-f_2)^2 + p_1\sigma_1^2 + (1-p_1)\sigma_2^2 \qquad (9)$$
$$p_1 = \frac{I_1}{I_1+I_2}$$

If we assume there is no cyclic variation in the widths of the individual components, σ_1, σ_2, or in the center frequency of the fast component, f_2, these parameters can be fixed to their mean values of 59.3 Hz, 87.1 Hz and 67.8 Hz respectively, obtained from the fit to the mean spectrum (Table I). Then the equations (9) can be rearranged to give a quadratic for p_1, with the total intensity $I_1 + I_2$, centroid f_0 and variance σ^2 used to calculate the individual component intensities and the center frequency of the Bragg component, f_1. These are shown on the right hand side of Fig. 9.

The intensity and center frequency of the Bragg component both exhibit a sinusoidal variation, almost in phase. Hence there is a strong correlation between center frequency and intensity for this component (Fig. 10), with a gradient of 57 Hz and an intercept of –62 Hz. This is shown as a solid black line in Fig. 7, with the center frequency of the fast component at 67.8 Hz shown as a dashed black line. Fig. 7 and Fig. 10 are not directly comparable, due to the differing amounts of averaging involved in their production, but it does seem plausible that the combined amplitude and frequency

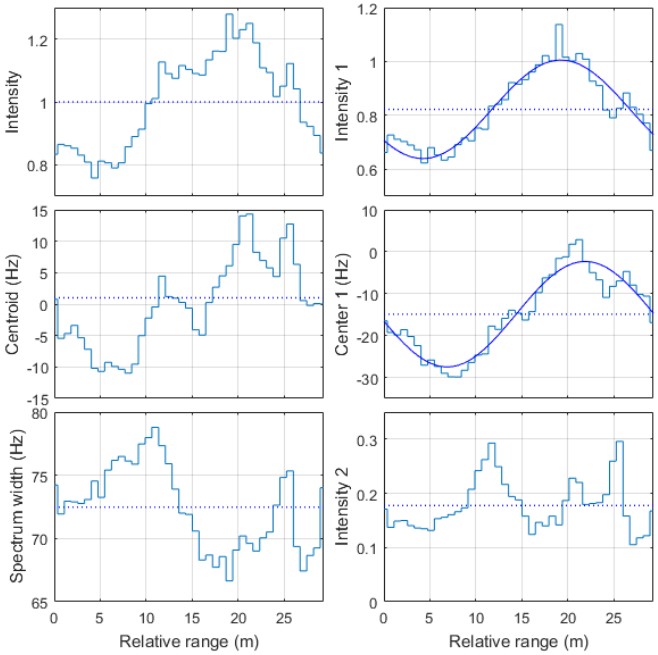

Fig. 9. Left, top to bottom: Intensity, centroid and width from the average Doppler spectrum over one swell wavelength, shown in Fig. 8. Right, top to bottom: Intensity and center frequency of the Bragg component and intensity of the fast component, calculated from the overall intensity, centroid and width using the method and assumptions described in the text. Dotted blue lines indicate the average in each plot. Blue curves are sinusoids fitted to the data.

modulation of the Bragg component is the explanation for the center frequency – intensity correlation in the overall spectrum.

The mean Doppler of the Bragg component is –14.9 Hz, indicated by the black dot in Fig. 10. This should correspond to the mean water surface velocity, which may not be zero, due to wind drift and currents. The true zero Doppler frequency is not known, so the spectrum was centered at the overall peak intensity in pre-processing (black square in Fig. 10). Looking up swell, the swell crest will occur at the maximum Doppler

center frequency. Comparing the center right and bottom right plots in Fig. 9, it can be inferred that the fast component peaks ahead of the swell crest, and again behind the crest. This causes the overall spectrum width to be out of phase with the overall intensity and center frequency. At the outset the two components were assumed to be uncorrelated, but in fact there is a weak correlation between the component intensities, with a correlation coefficient of 0.11. If it were possible to take the covariance into account, this would increase the shape parameter estimates for the fast scatter component.

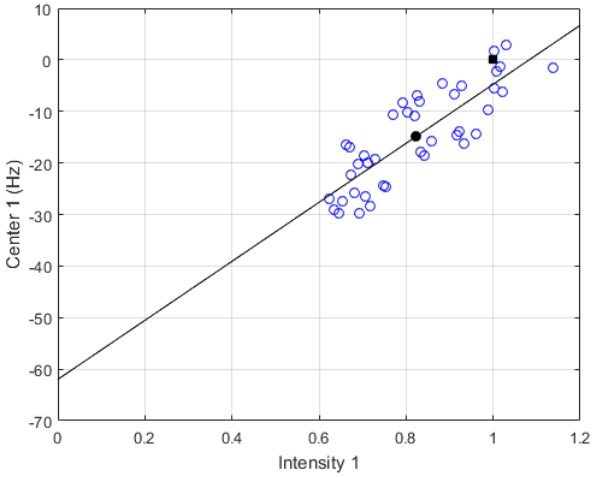

Fig. 10. Correlation between the center frequency and intensity of the Bragg component, HH polarization looking upswell. The black dot shows the mean Doppler and intensity of the Bragg component. The black square shows the arbitrary zero position of the Doppler frequency scale at a normalized intensity of 1.

V. CONCLUSION

A two component statistical model has been proposed for coherent sea clutter, with each component having its own spatial correlation. The model brings together several findings from previous work, such as the existence of separate Bragg and fast scattering components in the Doppler spectrum, the correlation between Doppler spectrum center frequency and intensity, and the variation in the second moments across the Doppler spectrum. Parameters for the two components can be estimated by simultaneous least squares fitting of the Doppler and variance spectra. The G2 distribution for the sum of two independent gamma variates with different shape and scale parameters is proposed as a texture model. Fitting the G2 PDF to the data provides another means to separate the two components.

The range variation of the two components is difficult to separate, but this was achieved for the HH polarization in the up swell direction, by cyclic averaging of the Doppler spectrum over the swell wavelength. The Bragg component shows sinusoidal variation in both intensity and Doppler frequency, leading to a correlation between the spectrum center frequency and intensity. The fast component peaks in intensity ahead of the swell crest and again behind the crest. This provides an alternative explanation for the fluctuations in overall spectrum width being out of phase with the fluctuations in center frequency and intensity, a feature of radar sea clutter previously attributed to thermal noise from the radar [15],[16].

This two component model is useful as an aid to understanding many of the features of sea clutter. With some further development it should be possible to simulate realistic coherent sea clutter from the model, which will be useful for the testing of signal processing and detection algorithms.

ACKNOWLEDGMENT

The author thanks Luke Rosenberg for useful discussions and assistance with the Ingara data.

REFERENCES

[1] L. B. Wetzel, Radar Handbook, 3rd ed. McGraw-Hill, 2008, ch. 15.

[2] R. J. Miller, “Variability in spectra of low-grazing angle sea clutter returns”, NATO/RTO Publications, Proceedings of SET Symposium on Low Grazing Angle Clutter: Its Characterisation, Measurement and Application, April 2000

[3] S. Watts, “Modeling and simulation of coherent sea clutter”, IEEE Trans AES vol. 48, no. 4, pp. 3303-3317, October 2012.

[4] S. Watts, L. Rosenberg, M. Ritchie and S. Bocquet, “The Doppler spectra of medium grazing angle sea clutter; part 1: characterisation”, IET Radar Sonar Navig., vol. 10, no. 1, pp. 24-31, 2016.

[5] S. Watts, L. Rosenberg, M. Ritchie and S. Bocquet, “The Doppler spectra of medium grazing angle sea clutter; part2: model assessment”, IET Radar Sonar Navig., vol. 10, no. 1, pp. 32-42, 2016.

[6] D. Walker, “Experimentally motivated model for low grazing angle radar Doppler spectra of the sea surface”, IEE Proc. Radar, Sonar & Navig., vol. 147, no. 3, pp. 114-120, June 2000.

[7] D. Walker, “Doppler modelling of radar sea clutter”, IEE Proc. Radar, Sonar & Navig., vol. 148, no. 2, pp. 73-80, April 2001.

[8] L. Rosenberg, “Characterization of high grazing angle X-band sea-clutter Doppler spectra”, IEEE Trans. AES, vol. 50, no. 1, pp. 406-417, January 2014.

[9] G. Davidson, “Simulation of coherent sea clutter”, IET Radar Sonar Navig., vol. 4, no. 2, pp. 168-177, April 2010. (Special Issue on Radar Clutter)

[10] S. Bocquet, L. Rosenberg and S. Watts, “Simulation of coherent sea clutter with inverse gamma texture”, International Conference Radar 2014, October 2014.

[11] M. McDonald and D. Cerutti-Maori, “Coherent radar processing in sea clutter environments, part 1: modelling and partially adaptive STAP performance”, IEEE Trans. AES, vol. 52, no. 4, pp. 1797-1817, August 2016.

[12] M. McDonald and D. Cerutti-Maori, “Multi-phase centre coherent radar sea clutter modelling and simulation”, IET Radar Sonar Navig., vol. 11, no. 9, pp. 1359-1366, 2017.

[13] L. Rosenberg and S. Bocquet, “Comparison of bi-modal coherent sea clutter models”, submitted to International Conference Radar 2018.

[14] S. Bocquet, “Parameter estimation for Pareto and K distributed clutter with noise”, IET Radar Sonar Navig., vol. 9, no. 1, pp. 104–113, 2015.

[15] S. Haykin, R. Bakker, and B. W. Currie, “Uncovering nonlinear dynamics – The case study of sea clutter”, *Proceedings of the IEEE*, vol. 90, no. 5, pp. 860-881, May 2002.

[16] M. Greco, F. Bordoni and F. Gini, "X-band sea clutter non-stationarity: the influence of long waves", IEEE Journal on Ocean Engineering, Special Issue on "Non-Rayleigh Reverberation and Clutter", vol.29, no. 2, pp. 269-283, April 2004.